The Astrophysical Journal Letters, 891:L10 (7pp), 2020 March 1 https://doi.org/10.3847/2041-8213/ab75ec

Onset of Cosmic Reionization: Evidence of an Ionized Bubble Merely 680 Myr after the Big Bang

V. Tilvi[1], S. Malhotra[2], J. E. Rhoads[2], A. Coughlin[3], Z. Zheng[4], S. L. Finkelstein[5], S. Veilleux[6], B. Mobasher[7], J. Wang[8], R. Probst[9], R. Swaters[6], P. Hibon[10], B. Joshi[1], J. Zabl[11], T. Jiang[1], J. Pharo[1], and H. Yang[1]
[1] School of Earth and Space Exploration, Arizona State University, Tempe, AZ 85287, USA; tilvi@asu.edu
[2] Astrophysics Science Division, Goddard Space Flight Center, Greenbelt, MD 20771, USA
[3] Chandler-Gilbert Community College, Chandler, AZ 85225-2499, USA
[4] CAS Key Laboratory for Research in Galaxies and Cosmology, Shanghai Astronomical Observatory, Shanghai 200030, People's Republic of China
[5] Department of Astronomy, The University of Texas at Austin, Austin, TX 78712, USA
[6] Department of Astronomy and Joint Space-Science Institute, University of Maryland, College Park, MD 20742, USA
[7] Department of Physics and Astronomy, University of California, Riverside, CA 92521, USA
[8] CAS Key Laboratory for Research in Galaxies and Cosmology, Department of Astronomy, University of Science and Technology of China, Hefei, Anhui 230026, People's Republic of China
[9] NOAO, 950 N. Cherry Avenue, Tucson, AZ 85719, USA
[10] European Southern Observatory, Alonso de Cordova 3107, Casilla 19001, Santiago, Chile
[11] Univ Lyon, Univ Lyon1, Ens de Lyon, CNRS, Centre de Recherche Astrophysique de Lyon UMR5574, F-69230 Saint-Genis-Laval, France
Received 2019 October 21; revised 2020 January 31; accepted 2020 February 12; published 2020 February 27

Abstract

While most of the intergalactic medium (IGM) today is permeated by ionized hydrogen, it was largely filled with neutral hydrogen for the first 700 million years after the big bang. The process that ionized the IGM (cosmic reionization) is expected to be spatially inhomogeneous, with fainter galaxies likely playing a significant role. However, we still have only a few direct constraints on the reionization process. Here we report spectroscopic confirmation of two galaxies and very likely a third galaxy in a group (hereafter EGS77) at redshift $z = 7.7$, merely 680 Myr after the big bang. The physical separation among the three members is <0.7 Mpc. We estimate the radius of ionized bubble of the brightest galaxy to be about 1.02 Mpc, and show that the individual ionized bubbles formed by all three galaxies likely overlap significantly, forming a large yet localized ionized region, indicative of inhomogeneity in the reionization process. It is striking that two of three galaxies in EGS77 are quite faint in the continuum, thanks to our selection using their Lyα line emission in the narrowband filter. Indeed, one is the faintest spectroscopically confirmed galaxy yet discovered at such high redshifts. Our observations provide direct constraints on the process of cosmic reionization, and allow us to investigate the properties of sources responsible for reionizing the universe.

Unified Astronomy Thesaurus concepts: Reionization (1383); Early universe (435); High-redshift galaxies (734); Lyman-alpha galaxies (978); Galaxy groups (597); Intergalactic medium (813)

1. Introduction

Cosmological simulations indicate that the process of reionization is expected to be spatially inhomogeneous (e.g., Furlanetto et al. 2004; Iliev et al. 2006; Zahn et al. 2007; Mesinger & Furlanetto 2008; Jensen et al. 2014), and started when intense UV radiation from individual galaxies or groups of galaxies first ionized their local surroundings and formed ionized bubbles of size $\simeq$1 Mpc, which later grew to fill the entire intergalactic medium (IGM), marking the end of the reionization process (Shin et al. 2008).

Star-forming galaxies at high redshifts are expected to have contributed to the reionization process (e.g., Bouwens et al. 2015; Finkelstein et al. 2015; Dayal & Ferrara 2018). These same galaxies, via their Lyα emission, provide a practical tool to study the reionization process (e.g., Malhotra & Rhoads 2004). Overdensities of Lyα galaxies have been discovered at $z \sim 7$ (Zheng et al. 2017; Castellano et al. 2018), which may indicate large ionized regions. Overdensities of bright Lyman-break galaxies have also been found at these redshifts (e.g., Trenti et al. 2012; Castellano et al. 2016; Harikane et al. 2019). We have carried out a unique narrowband (NB) imaging survey, the Cosmic Deep And Wide Narrowband survey (DAWN; PI: Rhoads), with enough sensitivity to detect Lyα emitting galaxies at a redshift of $z = 7.7$ and enough area coverage to detect the possible inhomogenieties and ionized bubbles expected at early stages of reionization. The NB technique has been proven successful at identifying $z > 6$ Lyα galaxies (Hu et al. 2010, 2019; Ouchi et al. 2010; Rhoads et al. 2012). Here we present a discovery of the most distant galaxy group (hereafter EGS77), identified using NB imaging, and confirmed via spectroscopic observations. The visibility of faint Lyα emission indicates an ionized IGM in the local vicinity of this group.

2. Imaging

2.1. Observations and Data Reduction

We obtained deep NB imaging observations of the Extended Groth Strip (EGS) field (R.A. 14:19:16 decl. +52:52:13), as part of the DAWN survey. This is a uniquely deep survey given its sensitivity as well as area coverage, with a primary objective of identifying galaxies at redshift $z = 7.7$. Here we present relevant details of the DAWN survey (Rhoads et al. 2020, in preparation, Coughlin et al. 2018). The DAWN survey was carried out using a custom narrowband filter (FWHM = 35 Å, central wavelength = 10660 Å), mounted on the NOAO Extremely Wide-Field InfraRed Imager (NEWFIRM; Probst et al. 2008) at the Kitt Peak 4 m Mayall telescope. The

NEWFIRM instrument has a wide field of view (28×28 arcmin^2) with a resolution of $0\farcs4$ per pixel. We obtained individual images with 600 s integration time and Fowler samples of 16 with 8 digital averages during the readout. To achieve clean sky background subtraction we used random dithering with a dither size of $45''$.

The data reduction was primarily done using the NEWFIRM data reduction pipeline (Swaters et al. 2009). However, to generate the final stack of all the images produced by the pipeline (sky subtracted, cosmic-rays cleaned, re-projected) we used our own scripts to remove bad frames that were visually inspected in order to maximize the signal-to-noise ratio (S/N) of astronomical objects. The final NB stack is equivalent to a total integration time of 67 hr, yielding a 5σ line flux sensitivity of $\sim 7 \times 10^{-18}$ erg s^{-1} cm^{-2}. To select high-redshift Lyα emission-line candidates we used this NB image as well as publicly available broadband images at visible wavelengths (*Hubble Space Telescope* (*HST*)/ACS F606W, F814W) and at near-IR wavelengths (*HST*/WFC3 F125W, F160W) and *Spitzer* IRAC images. These observations were taken as part of the GO10134 program (PI: M. Davis), GO12063 program (PI: S. Faber), and GO61042 program (PI: G. Fazio).

2.2. Selection of z = 7.7 Candidate Galaxies

To generate the source catalog we first aligned all images that include F606W, F814W, near-IR NB1066 (NB from DAWN survey), and near-IR broadband F125W, F160W images onto a common world coordinate system grid. We then used a source detection software (SExtractor; Bertin & Arnouts 1996) in dual image mode, where the detection image (in this case the NB) is used to identify the pixels associated with each object, while the fluxes are measured from the respective photometry image.

For robust selection of candidate galaxies at $z = 7.7$ we followed a set of criteria that has yielded a high spectroscopic success rate at $z = 4.5$ and 5.7 (Rhoads & Malhotra 2001; Rhoads et al. 2003; Dawson et al. 2004, 2007; Wang et al. 2009). Following this, each of our candidates had to satisfy all of the following criteria: (1) 5σ detection in the NB, (2) 3σ significant narrowband excess (compared to the F125W image), and (3) non-detection ($<2\sigma$) in the individual optical images (F606W, F814W). Criteria 1 and 2 ensure real emission-line sources, while criterion 3 eliminates most low-redshift sources. Using this set of criteria we identified three $z = 7.7$ candidates, z8_5, z8_4, and z8_SM, for spectroscopic follow-up. Formally, z8_SM has an NB S/N ~ 4 (just below our selection threshold); however, it has an aggregate S/N = 13 in NB+F125W+F160W. Given that it satisfied all other selection criteria, and given its proximity to other two galaxies, we included it for the spectroscopic follow-up observations. Galaxy z8_5 was independently identified as a Lyman-break galaxy by Oesch et al. (2015).

Figure 1 shows image cutouts of all three candidates in five filters. All three galaxies have significant fluxes in the NB filter, indicating the presence of strong emission lines, most likely Lyα lines at the observed wavelength of 1.066 μm. None of the galaxies have detectable fluxes at the visible wavelengths, suggesting that these galaxies are consistent with being at redshifts $z \geqslant 7$. All three galaxies are detected in both F125W and F160W (see Table 1), despite two of them being faint, making z8_4 the faintest galaxy discovered at such high redshifts, thanks to the NB selection technique in which detection of galaxies does not depend on the continuum brightness.

2.3. Photometric Redshifts and Spectral Energy Distributions

We use *EAZY* (Brammer et al. 2008) with spectral energy distribution (SED) templates that have emission lines (eazy_v1.3) along with broadband fluxes to derive the photometric redshift probability distribution $p(z)$. We allow a wide range of redshift grids ($z = 0.1$ to $z = 9$) to search for the best-fit SED template. In addition to the photometry (discussed in Section 2.2), we also used *HST*/WFC3 F105W photometry (GO:13792, PI: Bouwens) for z8_5 and CFHT-Y band photometry for z8_4 and z8_SM.

As shown in Figure 2, for all three galaxies the best-fit SEDs (shown in blue color) prefer spectral templates that correspond to a photometric redshift $z_{\rm phot} = 7.7$. This is also evident from the $p(z)$ (shown in the inset); the presence of strong emission lines in the NB filter yields tight constraints on the $p(z)$. For completeness, we also show the low-redshift galaxy templates (gray color), which are disfavored due to much larger χ^2 values of the SED fit. For the brightest galaxy z8_5 (previously identified in Oesch et al. 2015), the difference between the best-fit χ^2 value of the low-redshift template and high-redshift template is 86. For z8_4 and z8_SM, while the difference between the best-fit χ^2 value of the low-redshift template and high-redshift template is >1, it is not as high as that for z8_5 given their lower S/N. Furthermore, all three galaxies have large rest-frame Lyα equivalent widths EW$_{\rm rest} > 23$Å (see Table 1), which likely makes them visible as Lyα-emitting galaxies.

3. Spectroscopic Observations

To confirm the photometric redshifts of these galaxies, we performed *Y*-band spectroscopy using the Multi-Object Spectrometer for Infra-Red Exploration (MOSFIRE) spectrograph (McLean et al. 2012) on the Keck I telescope. The MOSFIRE instrument allows us to obtain spectroscopic observations of multiple objects simultaneously, with the *Y*-band covering Lyα lines redshifted to $z = 7$–8.2. We targeted three Lyα galaxy candidates in the EGS field as our primary science targets, and used low-redshift emission-line candidates as fillers. Observations were taken on 2017 May 6, with individual exposures having 140 sec integration time and *AB* pattern dither offsets along the slit, with offset of $\pm 1''$ from the center. The spectroscopic conditions were good, with a typical seeing of $\sim 0\farcs7$ and a total integration time of about 4 hr per object.

We reduced data using the public MOSFIRE data reduction pipeline. It performs standard data reduction procedures, including sky subtraction, rectification of the 2D spectra, and wavelength calibration. For a given object, it also produces a corresponding S/N and a sigma image. The final 2D science spectra have a spatial resolution of $0\farcs18$ per pixel and a dispersion of 1.086 Å per pixel. For absolute flux calibration of 1D spectra, we compared the measured line flux of z8_5 with the calibrated flux from Oesch et al. (2015), and converted instrumental flux (in counts) to the absolute flux. The conversion factor derived for z8_5 is then used to calibrate spectra of z8_SM and z8_4.

Figure 3 shows the final coadded 2D and 1D *Y*-band spectra of all three galaxies. As seen, both galaxies z8_5 and z8_4

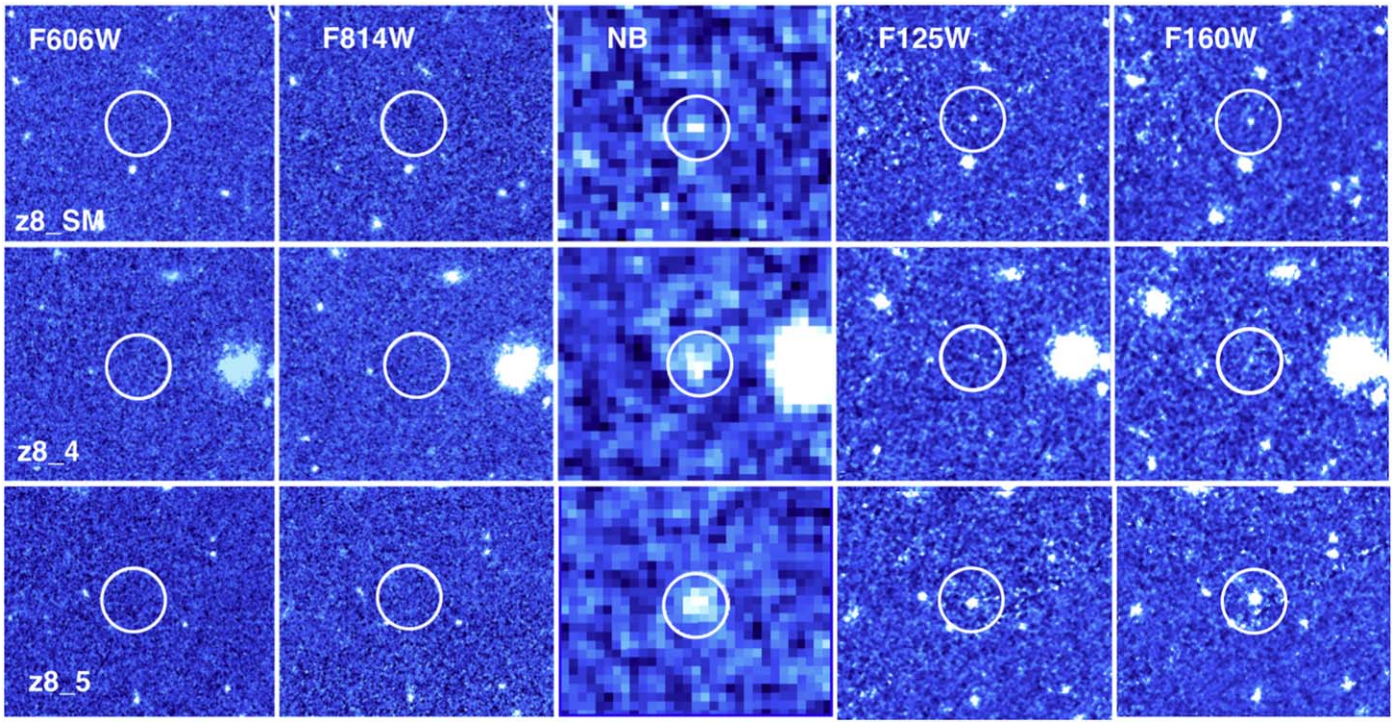

Figure 1. Image cutouts of all three members of EGS77. All galaxies are detected at redder wavelengths (NB, F125W, and F160W) but go undetected at the visible wavelengths (F606W and F814W). The sharp drop in the flux at visible wavelengths is consistent with the objects being at redshifts $z \geqslant 7$. All cutouts are $\sim 12''$ on the side, and the circles enclosing objects have $1\farcs4$ radii. NB images appear pixelated due to the coarser pixel resolution ($0\farcs4$ per pixel) compared with the much finer *HST* resolution ($0\farcs06$ per pixel). Bright fluxes in the NB images indicate the presence of strong emission lines.

Table 1
Photometry and Spectroscopic Measurements of EGS77

ID	R.A. J2000	Decl. J2000	F606W (mag)	F814W (mag)	NB (mag)	F125W (mag)	F160W (mag)
z8_SM	14:20:35.694	+53:00:09.318	<28.3[a]	<28.2[a]	24.76 ± 0.35	26.76 ± 0.13	26.66 ± 0.11
z8_4	14:20:35.169	+52:59:40.613	<28.3[a]	<28.2[a]	23.85 ± 0.15	27.25 ± 0.21	27.10 ± 0.16
z8_5	14:20:34.872	+53:00:15.242	<28.3[a]	<28.2[a]	23.60 ± 0.12	25.29 ± 0.03	25.08 ± 0.03

Spectroscopic Measurements

ID	z_{spec}	$f_{Ly\alpha}$ (erg s^{-1} cm^{-2})	EW_{rest} Å	$L_{Ly\alpha}$ 10^{43}(erg s^{-1})	H II Radii[b] pMpc	S/N (Lyα)	Distance[c] Trans	LoS
z8_SM	7.767	$0.29 \pm 0.06 \times 10^{-17}$	23 ± 6	0.2 ± 0.1	0.55	4.9	0.06	0.9
z8_4	7.748	$0.56 \pm 0.09 \times 10^{-17}$	71 ± 18	0.4 ± 0.1	0.69	6.0	0.09	0.2
z8_5	7.728	$1.70 \pm 0.14 \times 10^{-17}$	37 ± 3	1.2 ± 0.1	1.02	12.1	0.08	−0.5

Notes.
[a] $1\!2\sigma$ magnitude limits. All magnitudes are AB magnitudes.
[b] H II bubble radii based on Figure 15 from Yajima et al. (2018).
[c] Trans and LoS are the transverse and line-of-sight separation of each galaxy from the flux-weighted mean location of the group center, measured in pMpc.

show prominent emission lines (S/N > 5), while z8_SM has S/N = 4.9. In the following we show that these are very likely Lyα emission at $z = 7.7$.

For both z8_5 and z8_4, emission lines are free from the night sky OH lines, as shown in the shaded region (middle row). For z8_SM, while its emission line is close to a faint night sky line, given its higher S/N compared to the night sky lines, it is very likely a genuine emission line. Furthermore, the observed *Y*-position of the emission line in the 2D spectrum of z8_SM matches well with that expected based on the slit position in the mask (Figure 3 top panel), supporting our conclusion that this is a real emission line. We note that the presence of a faint night sky line at the position of the Lyα line may possibly affect the Lyα line flux measurements. However, given the faintness of the night sky line, we expect that it will have a minimal impact on the measurement of the Lyα line flux. In the following we demonstrate that these are very likely Lyα lines at $z = 7.7$.

One of the characteristics that distinguishes Lyα emission from star-forming galaxies and other emission lines is the line asymmetry (Rhoads et al. 2003) or *Skewness* (Kashikawa et al. 2006). To quantify the *Skewness* in the line, we calculated the weighted skewness parameter *Sw*, and found $Sw = 22 \pm 6$Å for z8_5. This confirms that z8_5 is a $z = 7.7$ galaxy because

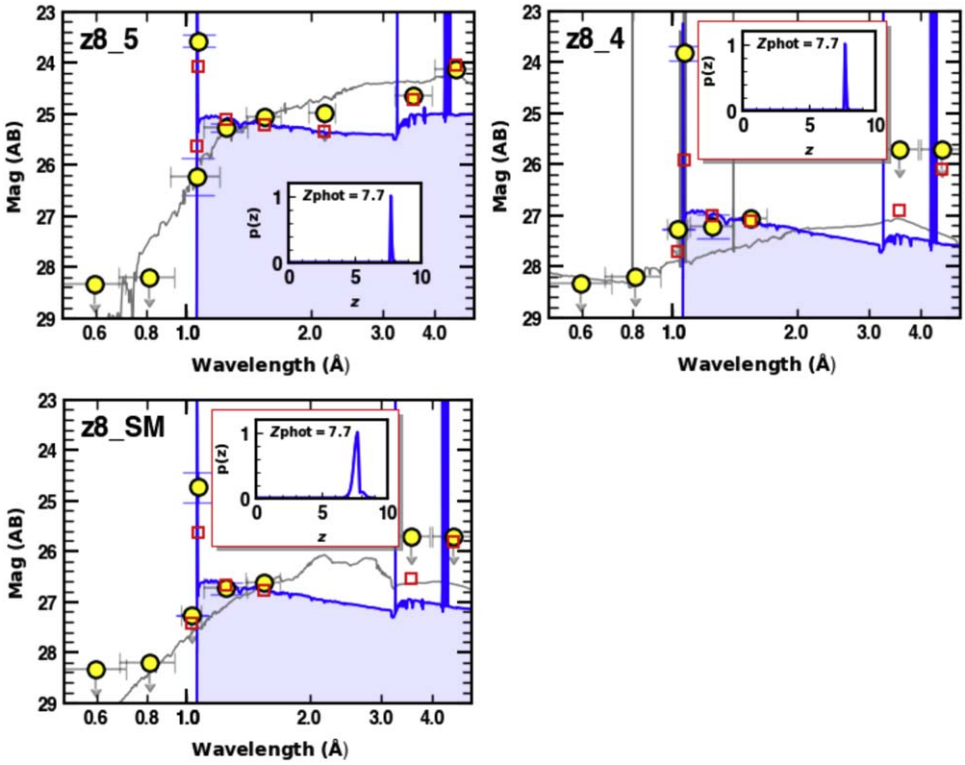

Figure 2. Spectral energy distributions (SEDs) of EGS77: SEDs based on fits to the photometry obtained from *HST*/ACS (F606W, F814W), NEWFIRM (NB), *HST*/WFC3 (F125W, F160W), and *Spitzer* IRAC (ch1, ch2). In addition, z8_5 photometry includes *HST*/WFC3 F105W observations, while z8_SM and z8_4 include CFHT-Y band photometry. The blue line represents the best-fit spectral template and the filled yellow circles represent photometric observations. Open squares indicate best-fit template fluxes convolved with the respective filters. Circles with downward pointing arrows represent 2σ non-detection limits. The best-fit photometric redshift distribution (shown in the inset) yields $z_{\rm phot} = 7.7$, which implies that there is a high probability of these galaxies being at high redshifts. For completeness, we also show low-redshift galaxy spectral templates (shown in gray color), which are disfavored given their larger χ^2 values.

$Sw > 3$Å is not seen in low-redshift emission lines of [O II], [O III], and Hα (Kashikawa et al. 2006). Indeed, z8_5 was previously identified as a Lyman-break candidate (labeled as EGS-zs8-1), and spectroscopically confirmed as a $z = 7.7$ galaxy (Oesch et al. 2015). Furthermore, recent *H*-band spectroscopic observations of this galaxy show the presence of a [C III] 1909 doublet (Stark et al. 2017). Thus, given all the evidence, z8_5 is unequivocally a Lyα-emitting galaxy at $z = 7.7$. For z8_4 the weighted skewness parameter for the observed emission line is $Sw = 17 \pm 7$ Å, confirming the line is Lyα at $z = 7.7$. For z8_SM, we cannot reliably measure the asymmetry of the line given its lower S/N in the spectrum. However, based on the best-fit SEDs, both z8_4 and z8_SM favor high-redshift solutions. Furthermore, if these were faint, low-redshift galaxies, the best-fit low-redshift SEDs imply a clear detection in the F606W and F814W filters. Thus, given all the evidence, z8_5 and z8_4 are unequivocally at redshifts $z = 7.728$ and $z = 7.748$ respectively, and z8_SM is also very likely at redshift $z = 7.767$.

It is striking that while z8_4 and z8_SM are faint ($M_{UV} > -20.3$ mag), both show Lyα emission lines. Moreover, despite the low number density of such faint galaxies at $z > 7$, all three galaxies are spectroscopically confirmed. This high spectroscopic success rate is likely because (1) our NB technique preselects galaxies with detectably strong line emission, and (2) EGS77 likely formed a large ionized bubble, allowing Lyα photons to escape. We discuss this in more detail in the following section.

4. Visibility of Lyα

The visibility of Lyα emission from star-forming galaxies at high redshifts depends on several factors including star formation rate, ionizing photon budget, galactic outflows, and proximity to ionized bubbles formed by other galaxies (e.g., Matthee et al. 2020). The star formation rate and the ionizing photon budget will directly influence the amount of ionized gas forming an ionized bubble, which in turn allows Lyα photons to travel unattenuated along the line of sight (Malhotra & Rhoads 2006). While there are arguments about whether fainter LBGs (Stark et al. 2011) or brighter LBGs (e.g., Matthee et al. 2020) are more likely to have a higher Lyα escape fraction, our observations (discussed below) show that perhaps the proximity to other galaxies with ionizing flux is the determining factor.

The separation between the most distant member z8_SM ($z = 7.767$) and z8_4 ($z = 7.748$) along the line of sight is about 0.7 pMpc (physical Mpc), which is the same as the separation between z8_4 and z8_5 ($z = 7.728$). In the transverse direction (i.e., projection on the sky) all three members are much closer to each other. The separation between z8_SM and z8_5 in the transverse direction is 10″ (0.05 pMpc), while the separation between z8_4 and z8_5 is 35″ (0.18 pMpc). Thus, given the proximity of all three galaxies with each other in both the transverse direction and along the line of sight, these galaxies will form a continuous attenuation-free path for Lyα photons if the radii of their ionized bubbles are $\geqslant$0.35 pMpc along the line-of-sight direction (Figure 4). This is because the ionized region is large

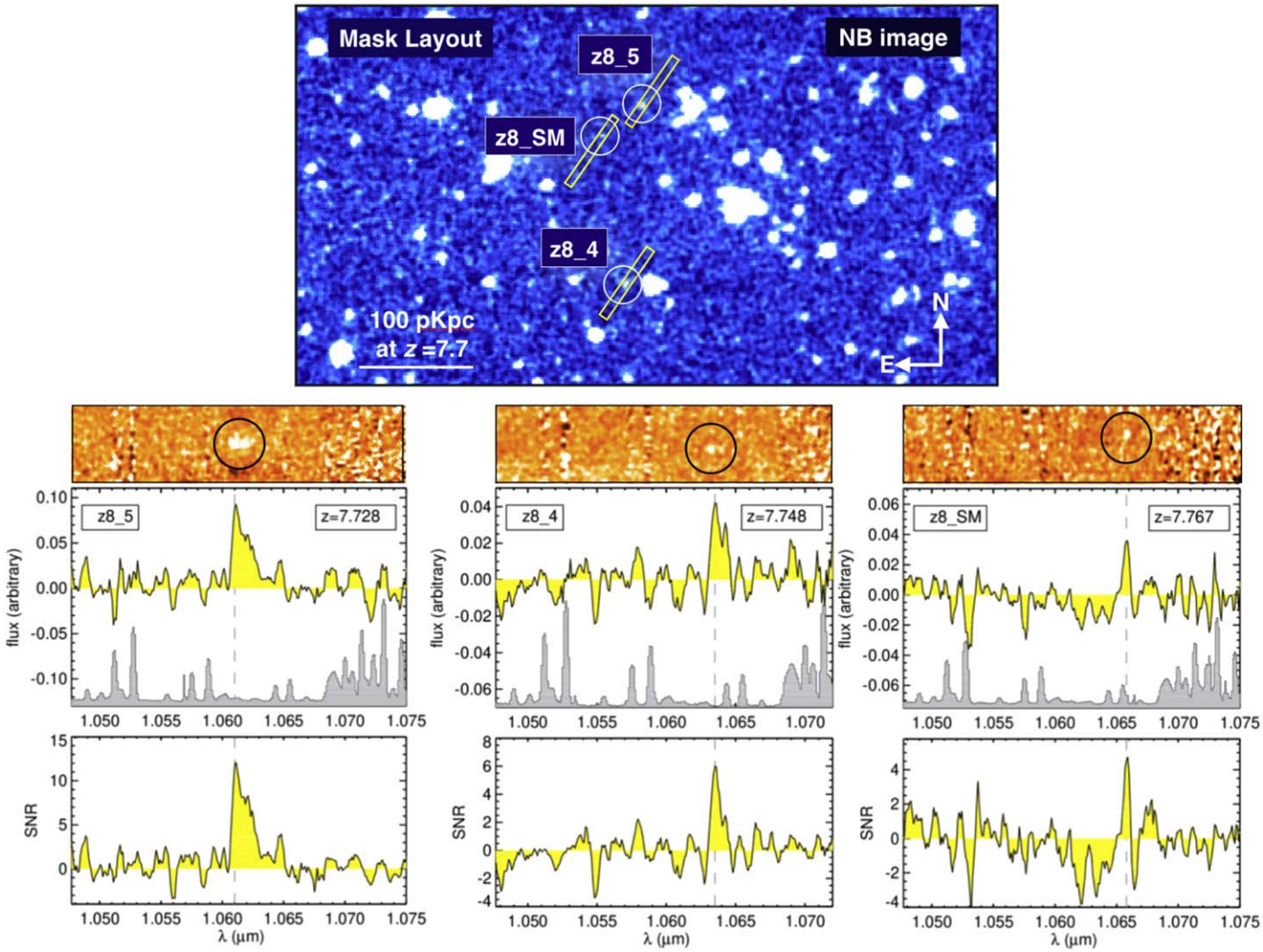

Figure 3. Spectroscopic observations of EGS77. Top: a portion of the EGS field centered on EGS77, and the multi-object mask layout used for MOSFIRE *Y*-band spectroscopic observations. The mask is overlaid on the NB image ($\sim 2\farcm3 \times 1\farcm2$), where the image is slightly smoothed for clarity. Lower panels: the top and middle rows show final stacked 2D and 1D spectra respectively, while the bottom row shows S/Ns. The maximum of the S/N is normalized to the total S/N of the Lyα line. The shaded gray region shows night sky lines with arbitrary normalization. Lyα lines (shown by black circles, and represented with vertical dashed lines in the middle row) are detected in all three galaxies at the expected observed wavelength of about 1.066 μm.

enough that the Lyα photons are redshifted by the time they reach the neutral hydrogen boundary, and thus can escape. This is supported by recent spectroscopic observations of the brightest galaxy z8_5, showing a [C III] 1909 doublet (Stark et al. 2017), which yields a velocity offset $\Delta V_{\mathrm{Ly}\alpha} = 340^{+15}_{-30}$ km s^{-1}. When compared to a FWHM = 360 km s^{-1} for this line (Oesch et al. 2015), it is implied that a substantial fraction of Lyα photons are leaving the galaxy at 340–520 km s^{-1}.

4.1. Estimation of Bubble Sizes

We now estimate the sizes of ionized bubbles formed by these galaxies, based on a theoretical model where the relation between Lyα luminosities and bubble sizes has been predicted through simulations, while the star formation rate is derived using the growth rate of halo mass with a constant tuning parameter (Yajima et al. 2018). The growth rate of halos is calculated using the halo merger trees based on an extended Press–Schechter formalism (Somerville & Kolatt 1999; Khochfar & Burkert 2001). These simulations reproduce the observed star formation rate density as well as the UV luminosity function of Lyman-break-selected galaxies at $z \sim 7$ and $z \sim 8$ (Bouwens et al. 2012). Next, to estimate the size of the ionized bubble, which is proportional to the ionizing photon budget, they used the star formation history of each halo using stellar population synthesis code STARBURST99 (Leitherer et al. 1999). Finally, the Lyα luminosity of each galaxy is calculated based on the number of ionizing photons absorbed within the galaxy. Photons that are absorbed will produce Lyα photons, while photons that escape cause cosmic reionization. Based on these simulations (Figure 15 from Yajima et al. 2018), the luminosity of our brightest galaxy z8_5 yields a radius of 1.02 pMpc for the H II bubble. For the remaining two galaxies z8_4 and z8_SM we find bubble sizes of 0.69 and 0.55 pMpc, respectively (see Figure 4). This implies that a substantial ionized region forms around brighter galaxies and galaxy groups (Matthee et al. 2020), through which Lyα photons can easily escape and hence be observed (Larson et al. 2018) even for faint galaxies with small Lyα velocity offset.

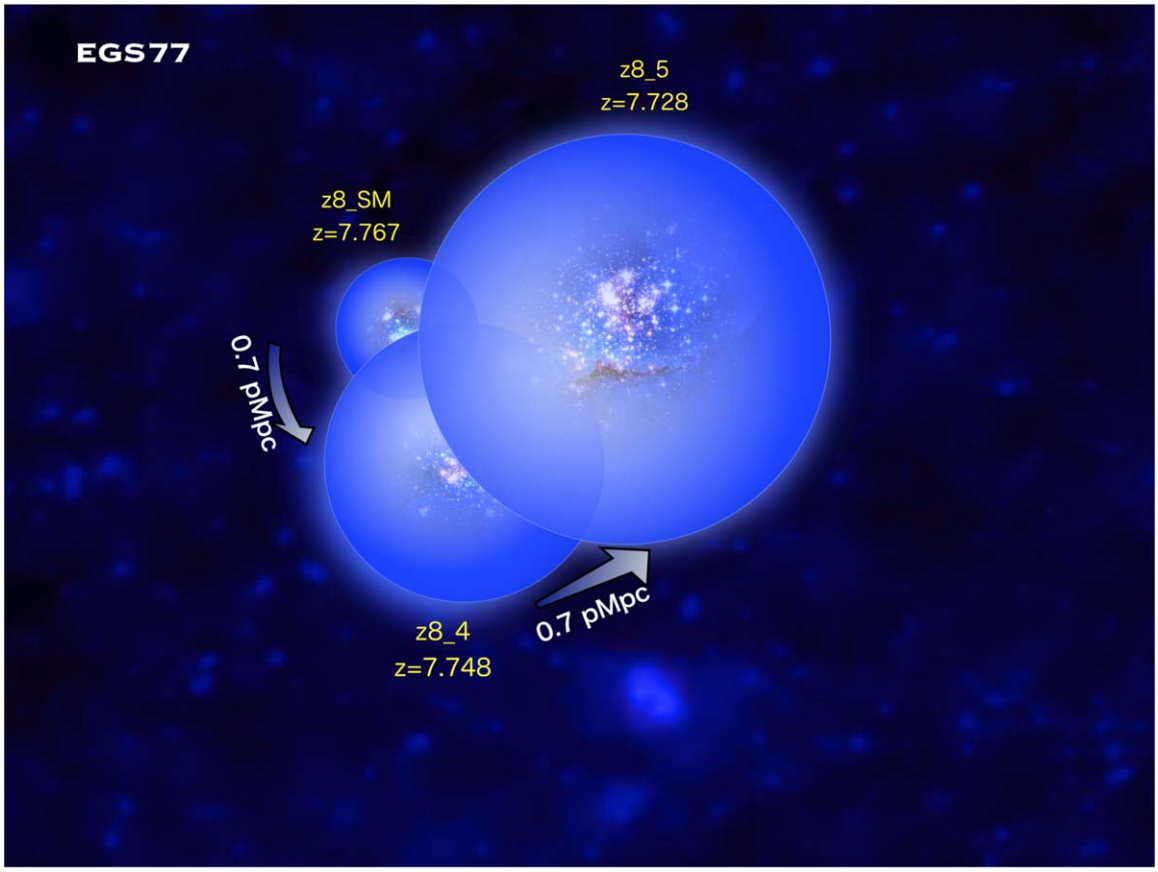

Figure 4. Rendition of the galaxy group EGS77 showing ionized bubbles formed by three galaxies near redshift 7.7. Galaxy z8_5 is the brightest, producing the largest ionized bubble, and lies in the front. It is estimated to produce an ionized bubble of radius 1 pMpc. The physical separation between each pair of galaxies is merely 0.7 pMpc along the line of sight, which implies that their ionized bubbles overlap substantially to create a continuous path allowing Lyα photons to escape.

5. Summary

In this Letter we report the discovery of the farthest galaxy group EGS77 at $z = 7.7$, merely 680 Myr after the big bang. EGS77 was initially identified using NB imaging observations from the DAWN survey, and later confirmed via spectroscopic observations using the MOSFIRE spectrograph on the Keck telescope. It is striking that all three galaxies in EGS77 are spectroscopically confirmed via Lyα emission line ($S/N_{Ly\alpha} \gtrsim 5$) despite two of them being faint in the continuum. In fact, EGS77 contains the faintest galaxy (in terms of the continuum brightness) discovered and spectroscopically confirmed at this redshift. Based on models and simulations from Yajima et al. (2018), we found that a large ionized bubble produced by the brightest galaxy z8_5 and two relatively smaller bubbles surrounding fainter galaxies, overlap significantly, producing a large yet localized ionized region.

At redshift $z = 7.7$, EGS77 is the most distant spectroscopically confirmed galaxy group yet identified. The associated bubble, implied by the prominent Lyα emission in all three spectra, is the most distant ionized bubble identified, and the first at a redshift where the bulk neutral hydrogen fraction is thought to approach or perhaps even exceed 50% (Robertson et al. 2015; Planck Collaboration et al. 2016; Finkelstein et al. 2019). This combination of local ionization at a redshift with substantially neutral bulk gas provides observational support for the picture of spatially inhomogeneous reionization that proceeds from the growth of ionized bubbles.

We thank the referee for many constructive comments that improved this manuscript. We thank the US NSF (Grant AST-1518057), and NASA for its financial support through the WFIRST Science Investigation Team program (NNG16PJ33C). Z.Y.Z. thanks the NSF of China (11773051) and the CAS Pioneer Hundred Talents Program. Data presented herein were obtained at the W.M. Keck Observatory, operated as a scientific partnership among Caltech, the University of California and the NASA. The Observatory was made possible by the generous financial support of the W.M. Keck Foundation. The authors wish to recognize and acknowledge the very significant cultural role and reverence that the summit of Maunakea has always had within the indigenous Hawaiian community. We are most fortunate to have the opportunity to conduct observations from this mountain.

ORCID iDs

V. Tilvi https://orcid.org/0000-0001-8514-7105
S. Malhotra https://orcid.org/0000-0002-9226-5350
J. E. Rhoads https://orcid.org/0000-0002-1501-454X
S. L. Finkelstein https://orcid.org/0000-0001-8519-1130
S. Veilleux https://orcid.org/0000-0002-3158-6820
P. Hibon https://orcid.org/0000-0003-3726-5494
B. Joshi https://orcid.org/0000-0002-7593-8584
T. Jiang https://orcid.org/0000-0002-2222-6129
J. Pharo https://orcid.org/0000-0003-2249-2539
H. Yang https://orcid.org/0000-0003-2260-7420

References

Bertin, E., & Arnouts, S. 1996, A&AS, 117, 393
Bouwens, R. J., Illingworth, G. D., Oesch, P. A., et al. 2012, ApJ, 754, 83
Bouwens, R. J., Illingworth, G. D., Oesch, P. A., et al. 2015, ApJ, 811, 140
Brammer, G. B., van Dokkum, P. G., & Coppi, P. 2008, ApJ, 686, 1503
Castellano, M., Dayal, P., Pentericci, L., et al. 2016, ApJL, 818, L3
Castellano, M., Pentericci, L., Vanzella, E., et al. 2018, ApJL, 863, L3
Coughlin, A., Rhoads, J. E., Malhotra, S., et al. 2018, ApJ, 858, 96
Dawson, S., Rhoads, J. E., Malhotra, S., et al. 2004, ApJ, 617, 707
Dawson, S., Rhoads, J. E., Malhotra, S., et al. 2007, ApJ, 671, 1227
Dayal, P., & Ferrara, A. 2018, PhR, 780, 1
Dewdney, P. E., Hall, P. J., Schilizzi, R. T., et al. 2009, IEEEP, 97, 1482
Finkelstein, S. L., D'Aloisio, A., Paardekooper, J.-P., et al. 2019, ApJ, 879, 36
Finkelstein, S. L., Ryan, R. E., Papovich, C., et al. 2015, ApJ, 810, 71
Furlanetto, S. R., Zaldarriaga, M., & Hernquist, L. 2004, ApJ, 613, 1
Harikane, Y., Ouchi, M., Ono, Y., et al. 2019, ApJ, 883, 142
Hu, E. M., Cowie, L. L., Barger, A. J., et al. 2010, ApJ, 725, 394
Hu, W., Wang, J., Zheng, Z., et al. 2019, ApJ, 886, 90
Iliev, I. T., Mellema, G., Pen, U.-L., et al. 2006, MNRAS, 369, 1625
Jensen, H., Hayes, M., Iliev, I. T., et al. 2014, MNRAS, 444, 2114
Kashikawa, N., Shimasaku, K., Malkan, M. A., et al. 2006, ApJ, 648, 7
Khochfar, S., & Burkert, A. 2001, ApJ, 561, 517
Larson, R. L., Finkelstein, S. L., Pirzkal, N., et al. 2018, ApJ, 858, 94
Leitherer, C., Schaerer, D., Goldader, J. D., et al. 1999, ApJS, 123, 3
Madau, P. 1995, ApJ, 441, 18
Malhotra, S., & Rhoads, J. E. 2004, ApJL, 617, L5
Malhotra, S., & Rhoads, J. E. 2006, ApJL, 647, L95
Matthee, J., Sobral, D., Gronke, M., et al. 2020, MNRAS, 492, 1778
McLean, I. S., Steidel, C. C., Epps, H. W., et al. 2012, Proc. SPIE, 8446, 84460J
Mesinger, A., & Furlanetto, S. R. 2008, MNRAS, 385, 1348
Oesch, P. A., van Dokkum, P. G., Illingworth, G. D., et al. 2015, ApJL, 804, L30
Ouchi, M., Shimasaku, K., Furusawa, H., et al. 2010, ApJ, 723, 869
Planck Collaboration, Adam, R., Aghanim, N., et al. 2016, A&A, 596, A108
Probst, R. G., Gaughan, N., Abraham, M., et al. 2004, Proc. SPIE, 5492, 1716
Probst, R. G., George, J. R., Daly, P. N., et al. 2008, Proc. SPIE, 7014, 70142S
Rhoads, J. E., Dey, A., Malhotra, S., et al. 2003, AJ, 125, 1006
Rhoads, J. E., Hibon, P., Malhotra, S., et al. 2012, ApJL, 752, L28
Rhoads, J. E., & Malhotra, S. 2001, ApJL, 563, L5
Robertson, B. E., Ellis, R. S., Furlanetto, S. R., et al. 2015, ApJL, 802, L19
Shin, M.-S., Trac, H., & Cen, R. 2008, ApJ, 681, 756
Somerville, R. S., & Kolatt, T. S. 1999, MNRAS, 305, 1
Stark, D. P., Ellis, R. S., Charlot, S., et al. 2017, MNRAS, 464, 469
Stark, D. P., Ellis, R. S., & Ouchi, M. 2011, ApJL, 728, L2
Steidel, C. C., Adelberger, K. L., Shapley, A. E., et al. 2003, ApJ, 592, 728
Stiavelli, M., Fall, S. M., & Panagia, N. 2004, ApJL, 610, L1
Swaters, R. A., Valdes, F., & Dickinson, M. E. 2009, in ASP Conf. Ser. 411, Astronomical Data Analysis Software and Systems XVIII, ed. D. A. Bohlender, D. Durand, & P. Dowler (San Francisco, CA: ASP), 506
Trenti, M., Bradley, L. D., Stiavelli, M., et al. 2012, ApJ, 746, 55
Wang, J.-X., Malhotra, S., Rhoads, J. E., Zhang, H.-T., & Finkelstein, S. L. 2009, ApJ, 706, 762
Yajima, H., Sugimura, K., & Hasegawa, K. 2018, MNRAS, 477, 5406
Zahn, O., Lidz, A., McQuinn, M., et al. 2007, ApJ, 654, 12
Zheng, Z.-Y., Wang, J., Rhoads, J., et al. 2017, ApJL, 842, L22